Applications in Engineering Science 7 (2021) 100062

Contents lists available at ScienceDirect

Applications in Engineering Science

journal homepage: www.sciencedirect.com/journal/applications-in-engineering-science

A simplified model for hydraulic fracturing and its role in seismicity

Antonio Giovinetto [a], Giordano Montegrossi [b,c], Lorenzo Fusi [*,a,c], Angiolo Farina [a], Fabio Rosso [a]

[a] Dipartimento di Matematica e Informatica "Ulisse Dini", Universitá degli Studi di Firenze, Viale Morgagni 67/a, Firenze 50134, Italy
[b] CNR-Institute of Geosciences and Earth Resources, Via G. La Pira, 4, Florence 50121, Italy
[c] INSTM - Consorzio Interuniversitario Nazionale per la Scienza e Tecnologia dei Materiali, Via G. Giusti 9, Firenze, Italy

ARTICLE INFO

Keywords:
Seismicity
Fracture theory
Westergaard solution

ABSTRACT

In this study we propose a simple mathematical model to evaluate the seismic energy (magnitude) generated by the injection of a pressurized liquid in a geothermal area. The aim is to distinguish between induced and triggered seismicity. We compute the induced seismicity by a simple equation that allows to evaluate the energy contribution of the human activity. By using the classical linear elastic fracture theory, we obtain a formula that correlates the strain energy to the injection pressure, to the material parameters of the rock under consideration and to the characteristic seismic length. We compare the results of the model with a series of recorded data available in the literature, showing that our model is capable of defining the maximum magnitude of seismic events caused by human activity. Consequently, the model puts in evidence the "triggered" events with larger magnitude that are produced by the elastic energy accumulated in the rocks at depth by other natural means (e.g. tectonic).

1. Introduction

The problem of evaluating the human contribution to the seismicity of a system during an exploitation/industrial activity and its impact in terms of induced seismicity has a long and complex history Evans et al. (2012); Foulger et al. (2018); Grünthal (2014); National Research Council (2013). Following McGarr et al. McGarr (2014), a distinction should be made between induced seismicity and triggered seismicity. In the former, the stress changes produced by human activity are comparable with the ambient stress acting on a fault. In the latter, the anthropogenic stress variation is only a small percentage of the natural tectonic stress field. Considering the difficulties in discriminating between induced and triggered seismic events, we use the term induced seismicity in a generic way for the two categories described above.

The possible occurrence of earthquakes induced by fluid re-injection activities is of public concern. However, many decades of production all around the world demonstrate that, with a few debated occurrences and excluding EGS (Enhanced/Engineered Geothermal Systems) experiments, induced seismicity related to geothermal activities is usually of small magnitude Evans et al. (2012); Foulger et al. (2018); Grünthal (2014); National Research Council (2013). In some cases, seismic events with magnitudes higher than 3 have been observed (e.g., M_L 4.4 at Berlin in El Salvador or M_L 3.4 at Basel Majer (2007); Zang (2014)).

Several factors influence the occurrence of induced earthquakes during geothermal energy operations. A first factor is the injection volume. Indeed, the larger is the volume of rock affected by stress changes, the larger is the number of events that are likely to occur. This is a first-order geometrical effect. Whether the size of the maximum possible event scales with the affected volume or with fault area is currently a debated issue Baisch et al. (2010); Gischig and Wiemer (2013); McGarr (2014). A second influencing factor is the type of system. In an ideal closed system, the operation will reach a steady-state condition and pore pressure changes will remain confined to a certain volume, so that the seismicity in such systems should level with time. In open systems, the pressure or strain footprint will increase with time, and seismicity will be more variable. These scenarios are possible when critically stressed patches are reached by the pressure/strain changes. Seismicity in such settings can be sporadic (Landau, Germany), increasing with time (Groningen Gas Field, The Netherlands) and almost steady (Paradox Valley, Colorado, USA). A third influencing factor is the depth of the system. Deeper systems are generally believed to produce more earthquakes, a consequence of the strength profile of the earth crust. Differential stresses increase with depth, while natural earthquakes are less frequent in the first three kilometers of the earths crust. Seismic theory suggests that the increase in seismogenic response due to the increase in depth overcomes the decay (see Gischig and Wiemer

* Corresponding author.
E-mail address: lorenzo.fusi@unifi.it (L. Fusi).

https://doi.org/10.1016/j.apples.2021.100062
Received 25 June 2021; Accepted 3 August 2021
Available online 11 August 2021

(2013); Hirschberg et al. (2015)). However there is surprisingly little empirical evidence about the depth dependence. A fourth important factor to consider is the pore pressure change. In this regard, the higher and the more rapid is the (differential) pore pressure changes, the more likely are induced events. Seismicity starts only after pressure changes have exceeded a certain minimum threshold. On the other hand, it is known that even small pore pressure changes can trigger faults very close to failure Rothert et al. (2003). A fifth and final factor to be taken into account is the nearness to critically pre-stressed and extended seismogenic faults. In this paper we indeed present a simple mathematical model aimed at estimating the seismic energy (magnitude) due to an event generated by the injection of a liquid at high pressure.

Currently, the estimate of the released energy is essentially based on the classic fracture model Griffith (1921); Perez (2004), whose opening is caused by a far-field tensile stress σ_o. The elastic energy is then estimated by simply replacing σ_o with the injection pressure. However, this procedure has no physical justification sice the fracture evolution is evidently generated by the pressurized fluid injected inside it, and not by a tensile stress applied to the edges of the medium and, in any case, very far from the fracture.

In this paper we develop a mathematical model that is exempt from this physical inconsistency as it considers the fracture opening caused by the liquid pressure inside the fracture and is thus able to estimate the release of deformation energy in terms of the injection pressure. The model depends on parameters such as the scale characteristic fracture length, the elastic modulus and Poission ratio of the rock under consideration. For each value of the injected pressure we compute the magnitude of the corresponding seismic event that can be compared with the magnitude recorded in situ. Some significant approximations have been introduced to obtain a mathematically tractable model. For example, the medium is assumed to be isotropic and homogeneous and a single flat slit is considered. This is a very schematic description, since in practice the presence of many fractures (possibly interconnected) and the medium inhomogeneities make the dynamics much more complex. However, this may seem like an excessive approximation, but in reality it is largely justified by the fact that problems like this are characterized by a great uncertainty of the data.

To assess the validity and the efficiency in defining a boundary between induced (antropic contribution only) and triggered seismicity, we compare the data of three case studies (Basel, Switzerland; Latera and Cesano in Latium region, Italy) with the results provided by the mathematical model. The case studies here presented are selected because of their clear attribution of the events and the related dataset. Data available in the literature include the recording of seismic events and the well head pressure, which, when added to the hydrostatic pressure, gives the injection pressure. Moreover, the elastic properties of rocks are known (elastic modulus and Poisson ratio) and the characteristic fracture length can be easily estimated exploiting a classical theoretical framework. Indeed, since the fracture opening occurs at the medium sound velocity, we can correlate the characteristic fracture length as the characteristic seismic length, that is known for the case studies considered here. All the data are reported in Häring et al. (2008) for Basel, Switzerland, and in Batini et al. (1980a, 1980, 1980b); Moia et al. (1993) for Latera and Cesano, Italy. We finally discuss conclusions and perspectives that the mathematical model offers in the interpretation of seismic phenomena. In particular, we evaluate the antropic contribution to the "instantaneous" energy release of the system and compare it with the measured seismic activity.

It is important to stress the fact that the theoretical framework of this work differs substantially from the one of Griffith (1921), since here the energy release is due to the injection pressure P_{in} and not to a generic stress σ_o acting on the external boundary of the physical domain. In addition, the fracture length in our model is essentially the characteristic seismic length (a parameter that can inferred from seismic signals). We shall see that, although our model provides results which are pretty similar to those of Griffith (1921), the physical framework on which those results are based upon rests on a more solid base that justifies its use.

2. Mathematical modeling

We develop the mathematical model making use of the classical linear elastic stress analysis of cracks (see Zehnder (2012)). The investigation of the released seismic energy is based on the evaluation of the forces acting at the crack tip, where the stress field can be decomposed in three modes called Mode I, Mode II and Mode III. In Mode I the crack opens orthogonally producing a tension/compression on the surface of the crack. In Mode II, III the surfaces of the crack slide one over the other producing shear stresses that act parallel to the surfaces. Since we are considering a "fluid pressure" as the driving force in the generation of strain energy, it is reasonable to focus on Mode I and to assume that the fluid exerts a normal force on the surfaces of the crack. If we assume that the fluid is also capable of exerting shear stresses comparable with the injection pressure (i.e. we consider Modes II, III), we can estimate seismic energy following an approach very similar to the one here illustrated for Mode I. Actually, we find that, "ceteris paribus", the calculated seismic energy is close to the one of Mode I. We schematize the problem of the injection of a fluid at high pressure as in Fig. 1 where the system is represented by a 2D domain with a 1D fracture of length $2a$. The stress tensor $\mathbf{S}$ has only three significant components:

$$\mathbf{S} = \begin{pmatrix} \sigma_1 & \tau \\ \tau & \sigma_2 \end{pmatrix},$$

and must satisfy the following boundary conditions

$$\mathbf{S}|_{\infty} = 0, \qquad \pm \mathbf{S}\mathbf{j}|_{\mathscr{F}} = \pm P_{\text{in}}\mathbf{j}, \tag{1}$$

where $\mathscr{F} = \{y = 0,\ -a \le x \le a\}$ represents the fracture, $\mathbf{j}$ is the unit vector of the y axis and where P_{in} is the pressure of the fluid within the crack. Notice that (1) implies zero traction on the external boundary and that the normal stress in the fracture is only due to the injected liquid. The linear elastic energy density is

$$e = \frac{1}{2}\begin{pmatrix} \sigma_1 & \tau \\ \tau & \sigma_2 \end{pmatrix} \cdot \begin{pmatrix} \varepsilon_1 & \gamma/2 \\ \gamma/2 & \varepsilon_2 \end{pmatrix}, \tag{2}$$

where ε_1, ε_2, γ are the components of the strain tensor, i.e.

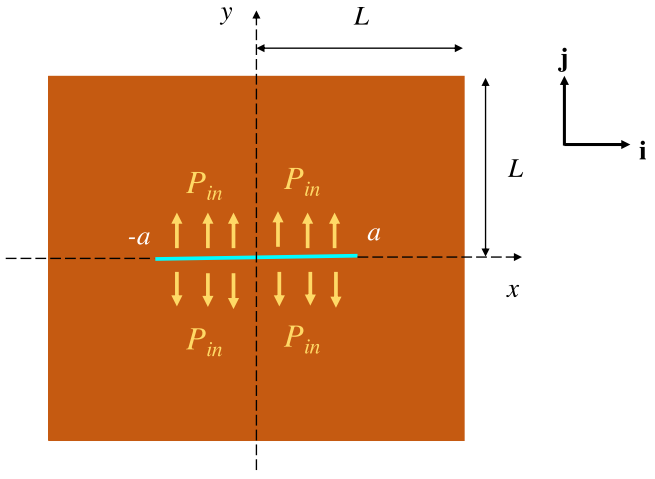

Fig. 1. Sketch of the fracture.

$$\begin{cases} \varepsilon_1 = \dfrac{1+\nu}{E}\Big[(1-\nu)\sigma_1 - \nu\sigma_2\Big], \\ \varepsilon_2 = \dfrac{1+\nu}{E}\Big[-\nu\sigma_1 + (1-\nu)\sigma_2\Big], \\ \gamma = 2\dfrac{1+\nu}{E}\tau, \end{cases} \tag{3}$$

E being the Young modulus and ν the Poisson ratio. From (2), (3) we get

$$e = \frac{1-\nu^2}{2E}\left[\left(\sigma_1^2+\sigma_2^2\right) + 2\left(\tau^2 - \nu\sigma_1\sigma_2\right)(1-\nu)^{-1}\right]. \tag{4}$$

The total energy of the system is obtained integrating over the physical domain

$$\mathscr{E} = \frac{1-\nu^2}{2E}\int_{-L}^{L}\int_{-L}^{L}\left[\left(\sigma_1^2+\sigma_2^2\right) + 2\left(\tau^2 - \nu\sigma_1\sigma_2\right)(1-\nu)^{-1}\right]dxdy, \tag{5}$$

where L is supposed to be sufficiently large compared to a, i.e. $L \gg a$. Because of symmetry it is easy to see that the integrand in (5) is even in x and y, so that the total energy relative to a single crack tip is

$$\mathscr{E} = \frac{2(1-\nu^2)}{E}\int_{0}^{L}\int_{0}^{L}\left[\left(\sigma_1^2+\sigma_2^2\right) + 2\left(\tau^2 - \nu\sigma_1\sigma_2\right)(1-\nu)^{-1}\right]dxdy. \tag{6}$$

The stress components σ_1, σ_2, τ can be determined using the Westergaard approach Zehnder (2012), in which the components are written using a single analytical function Z of complex variable $z = x + iy$. For mode I we have

$$\begin{cases} \sigma_1 = \mathscr{R}e(Z) - y\,\mathscr{I}m(Z'), \\ \sigma_2 = \mathscr{R}e(Z) + y\,\mathscr{I}m(Z'), \\ \tau = -y\,\mathscr{R}e(Z'), \end{cases} \tag{7}$$

where $\mathscr{R}e$ and $\mathscr{I}m$ denote, respectively, the real and imaginary part. The unique complex analytical function that satisfies (1) is

$$Z = P_{\text{in}}\left[1 - \frac{z}{\sqrt{z^2-a^2}}\right]. \tag{8}$$

We scale z with a and $Z, \sigma_1, \sigma_2, \tau$ with P_{in} and we identify the non dimensional variables with a "tilda", so that

$$\widetilde{Z} = \left[1 - \frac{\widetilde{z}}{\sqrt{\widetilde{z}^2-1}}\right], \qquad \widetilde{Z}' = \frac{1}{(\widetilde{z}^2-1)^{3/2}}. \tag{9}$$

The energy (6) can be rewritten as

$$\mathscr{E} = \frac{2(1-\nu^2)a^2P_{\text{in}}^2}{E}\underbrace{\int_0^{L/a}\int_0^{L/a}\left[\left(\widetilde{\sigma}_1^2+\widetilde{\sigma}_2^2\right) + 2\left(\widetilde{\tau}^2 - \nu\widetilde{\sigma}_1\widetilde{\sigma}_2\right)(1-\nu)^{-1}\right]d\widetilde{x}d\widetilde{y}}_{I}, \tag{10}$$

where I represents the total non dimensional energy. The integrand function in (10) is singular at the crack tips - see Fig. 2 for a graphical representation of the non dimensional stress components and the non dimensional energy density in Mode I - and tends to zero at infinity. The singularity at the tips is nevertheless integrable (see Zehnder (2012) for the proof) and factor I in (10) is bounded and tends to a positive constant value for $L \to \infty$. The value of I with $\nu = 0.26$ (typical of the systems studied in this article) is thus obtained selecting L/a sufficiently large. The numerical evaluation of the constant I gives

$$I = 1.5638. \tag{11}$$

In mode II, (7) is replaced by

$$\begin{cases} \sigma_1 = 2\mathscr{R}e(Z) - y\,\mathscr{I}m(Z'), \\ \sigma_2 = y\,\mathscr{I}m(Z'), \\ \tau = -\mathscr{I}m(Z) - y\,\mathscr{R}e(Z), \end{cases} \tag{12}$$

and (8) is replaced by

$$Z = iP_{\text{in}}\left[1 - \frac{z}{\sqrt{z^2-a^2}}\right]. \tag{13}$$

Substitution into (10) yields $I = 1.5849$, i.e. a value which is very similar to that of mode I, see (11). The non dimensional value of I for mode III cannot be calculated via Westegaard approach. In that case the momentum equation can be solved only numerically, providing the stress within the selected region. Also for mode III the energy I does not differ significantly from those of modes I, II.

Equation (10) is used to compute the seismic energy (expressed in *Joule*) with I given by (11). Finally the energy is converted into magnitude M_L via the Richter formula (see Gutenberg and Richter (1956))

$$\log_{10}\left(\frac{\mathscr{E}}{1\ Joule}\right) = 4.8 + 1.5M_L. \tag{14}$$

2.1. Comparison with classical approaches

To distinguish our approach from the classical methods in which the energy release is due to the application of a far field tension, we consider the historical energetic approach due to Griffith, Griffith (1921). Let Γ be the potential energy of the system and let $2a\gamma_s$ be the energy required to create the crack (γ_s is a material parameter representing the required energy per unit length). The total change in potential energy must be equal to the energy dissipated to propagate the crack

$$G = -\frac{d\Gamma}{da} = 2\gamma_s, \tag{15}$$

where G is the so-called energy release. The Griffith's criterion states that the crack may propagate if $G \geq 2\gamma_s$. The crucial point in the Griffith's theory is the evaluation of the potential energy Γ and the parameter γ_s. The main difference with our approach lies in the evaluation of the elastic energy that in our case is due to the force exerted by the fluid injected into the fracture. Indeed, following the standard approach Perez (2004), Γ is computed considering the plane deformation of an infinite plate subjected to a constant biaxial load σ_o applied at the margins of the domain Perez (2004), that is

$$\Gamma = \frac{\pi}{2}\frac{(1-\nu^2)\sigma_o^2a^2}{E}. \tag{16}$$

Though the analogies with the expressions for $\mathscr{E}$ are evident, in our model, consistently with what physically occurs, the injection pressure (and not the external biaxial loading) causes the increment in the strain energy. Further, in our case, the geometrical factor $\pi/2$ is replaced by the integral of the non dimensional energy. We also remark that our model is based on a theoretical framework that differs from the one of Griffith (1921). Indeed, we are dealing with a pressure P_{in} and not with a generic stress σ_o as in (16), which, at least in principle, has no relation with P_{in}. Moreover, the fracture length in our case is identified with the characteristic seismic length (a parameter that can be easily identified on the basis of seismic signals). In conclusion we can state that, though equation (10) and equation (16) yield similar numerical result, equation (10) has a sound physical base that justifies its use.

3. Case studies and discussion

In this section we analyze three case studies for which recorded data of seismic magnitude are available. They are C1: Basel, Switzerland; C2: Latera, Latium, Italy; C3: Cesano, Latium, Italy. Data for C1 are taken from Häring et al. (2008), while C2 and C3 are taken from Batini et al. (1980a, 1980, 1980b); Moia et al. (1993). The first data series are particularly numerous, while the other two are less. For each case we plot the recorded magnitude of seismic events (green) relative to a

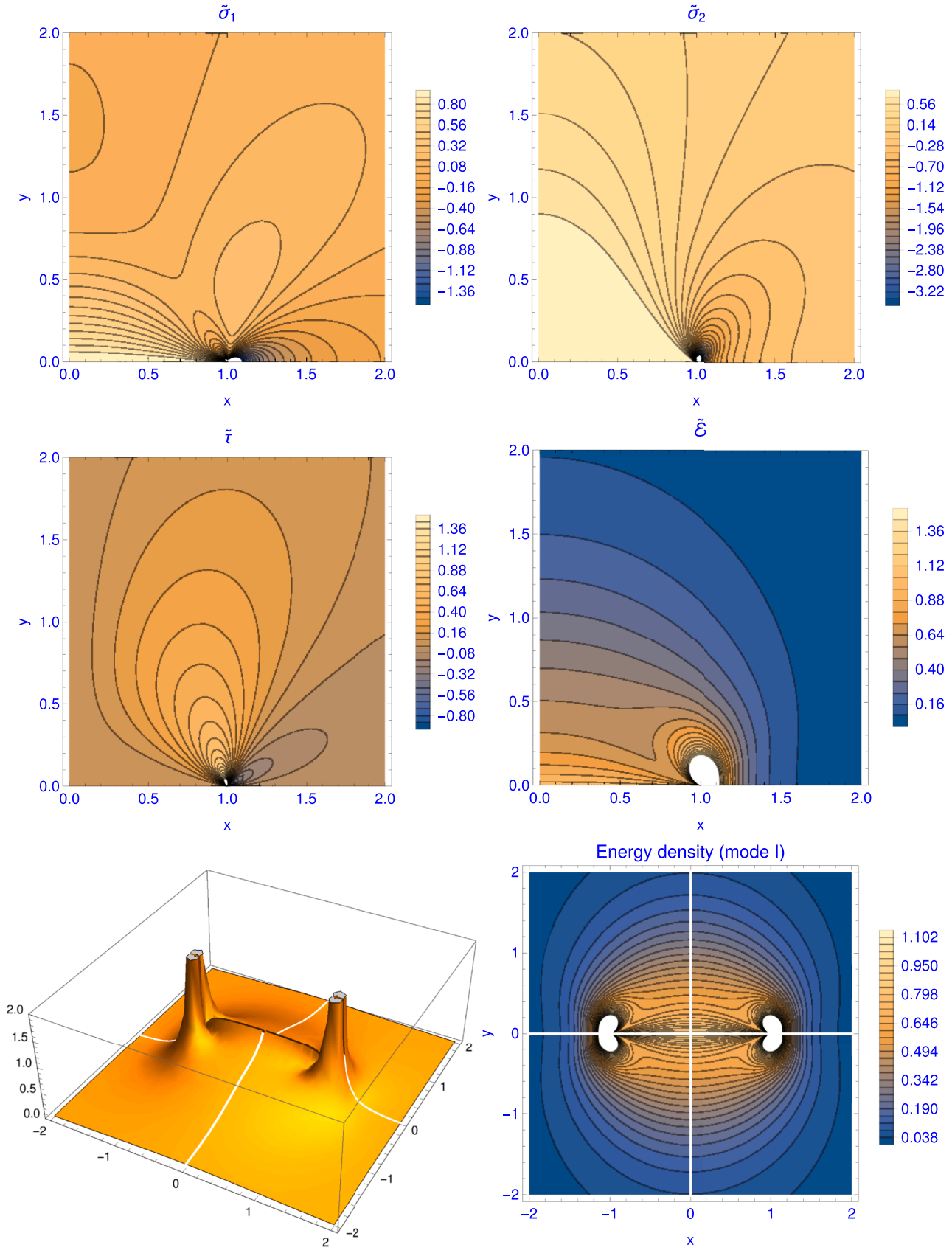

Fig. 2. Non dimensional stress components $\tilde{\sigma}_1$, $\tilde{\sigma}_2$, $\tilde{\tau}$, strain and energy density in mode I for $\nu = 0.26$.

certain time (reported on the x axis) and for a given injection pressure (red) and we also plot the magnitude predicted by the model (blue). The magnitude scale is placed on the left y axis, while the pressure scale is placed on the right y axis. We notice that the monotonicity of the calculated magnitude (blue) and of the pressure (red) is always the same, as expected.

The graphs displayed in Figs 3, 4, 5 show how the model (blue) essentially predicts the maximum values of the induced seismicity. Indeed the blue plot is almost always above the green bullets that represent the recorded events. Only in the Basel case we observe that some data are placed well above the prediction of the mathematical model. These are the values ranging in the interval $[2.5, 3.4]$ M_L, which are clearly due to triggered seismicity, as indicated in Häring et al. (2008). The data of case C2, reported in Fig. 4, are part of the injection tests carried out at RC1 well (Cesano) in which the seismic events - whose maximum magnitude is correctly predicted by our model - can be correlated with the injection pressure as stated in Batini et al. (1980b).

A similar situation is the one of L2 well (Latera) reported in Fig. 5 in which the seismicity is induced by the pumping operations, as reported in Batini et al. (1980b). Once again, our model provides the expected maximum magnitude in good agreement with field observations. Generally speaking, we notice an initial delay between the injection operations and the seismic response. This may be due to several factors, such as the presence of a pressure threshold for the onset of the response and/or a loading period of the system.

Whether maximum possible event size also scales with the affected volume or fault area is currently a debated issue but it is generally assumed that the injected volume of fluids is proportional to the number of events, rather than their magnitude Baisch et al. (2010); Gischig and Wiemer (2013); McGarr (2014). The seismic and the hydraulic energy clearly depend on the injected fluid volume De Barros et al. (2019), even though in our model this aspect is not taken into account. A large discrepancy, partly related to aseismic deformation, rock inhomogeneities and other effects, may also be present. The coupling between injected fluid volume and pressure is mainly due to the reservoir dynamics, and it is not really possible to have a clear separation between them, as the overall behavior of the system can only be modeled using a fully coupled 3D thermo-hydro-mechanical model Zbinden et al. (2017). In this paper we do not discuss the relation between the injected volume of water and the number of seismic events, two phenomena that are known to be correlated by at least the hydraulic properties of the system, and many possible loading factor (e.g. undersaturated rocks, pore expansivity, fracture opening etc.), but we propose a reformulation of the classic elastic theory to provide a simple method to evaluate the possible induced seismicity before field operations take place.

4. Conclusions

We have presented a simple mathematical model for determining the energy released by a seismic event that is induced by the injection of a liquid at high pressure. The model calculates the elastic strain energy due to the action of the pressurized liquid on the fractures present in the area of injection. The potential strain energy relative to a specific injection pressure is obtained assuming that the stress-strain relation is linear and expressing the energy density by means of the so-called Westegaard approach. The comparison of the model predictions with the data collected in situ has shown that our model is capable of providing the maximum induced seismic magnitude, defining a boundary between the antropic contribution and the triggered seismic events. We also remark that in the absence of triggered seismicity, the recorded data are generally below or equal to the values predicted by the mathematical model. Indeed, the latter estimates the maximum magnitude for the induced seismicity but there can be many reasons for which the natural system shows lower magnitude values. The many uncertainties in determining the effective overpressure at the fracture, in estimating the values of the elastic properties of the rocks and in calculating the characteristic seismic length reflect on the computed maximum magnitude, producing errors that are difficult to estimate. In terms of absolute error, the data used in the presented case studies sum up to less than 20% error on the energy, that is less than 0.1 in magnitude for the magnitude range considered. Based on the distinction between induced and triggered seismicity, the latter should have an energy by far greater than the antropic contribution. Considering the possible error in the energy release evaluation associated with our equation, we can define as triggered all the events that have energy at least one order of magnitude larger than the energy computed for the antropic contribution according to equation (16). We conclude that our model is effectively capable of providing the maximum boundary of the expected magnitude for the induced seismicity. In the data presented in Fig. 3, 4, 5, only the triggered events in the Basel case are significantly higher than the computed limit. With this in mind, equation (16) is a very useful and reliable tool to estimate a priori the seismic energy (which could therefore be easily converted into induced seismicity) due to fluid injection, i.e. caused by anthropogenic activity.

Declaration of Competing Interest

This manuscript has not been submitted to, nor is under review at, another journal or other publishing venue. The authors have no

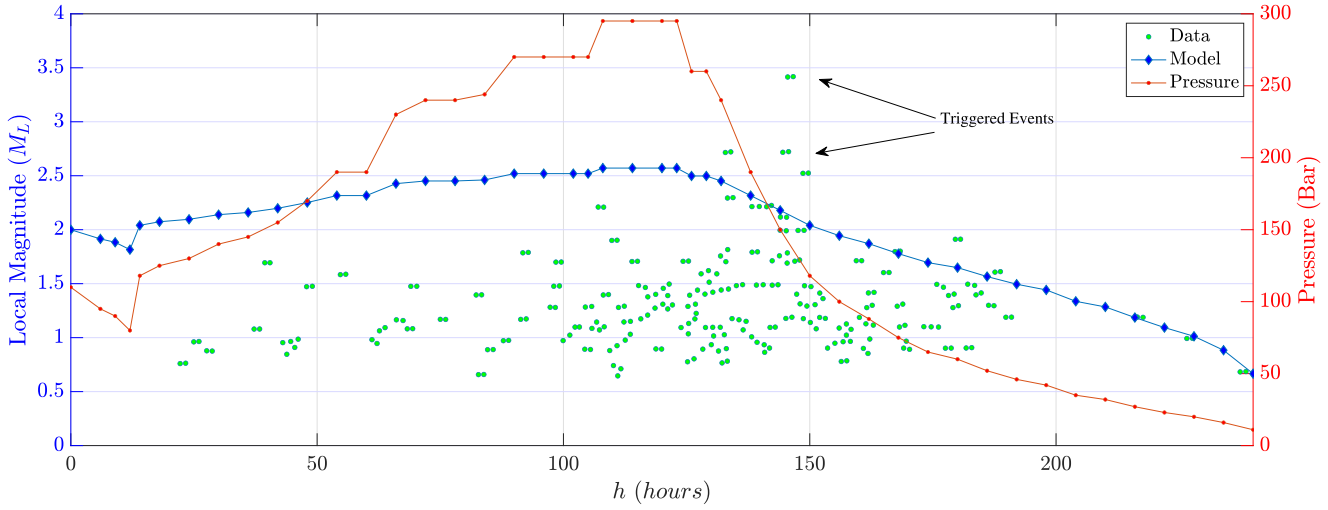

Fig. 3. Case C1: Basel, Switzerland. Initial date: 02 Dec 2006. $E = 20$ GPa, $\nu = 0.26$, $a = 60$ m.

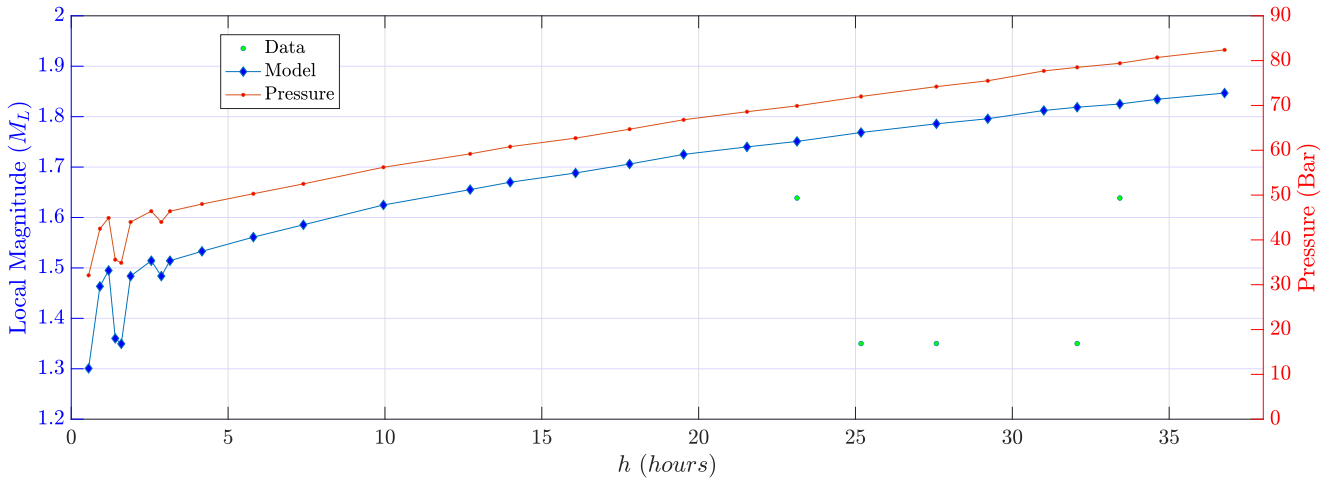

Fig. 4. Case C2: Cesano in Latium region, Italy. Initial date: 15 May 1978. $E = 30$ *GPa*, $\nu = 0.26$, $a = 75$ *m*.

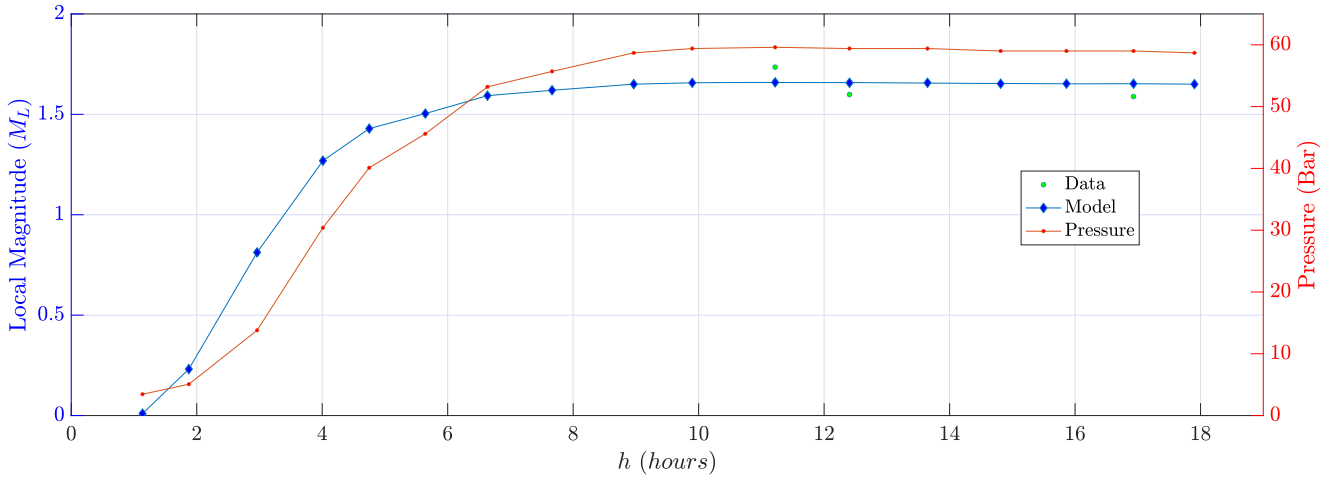

Fig. 5. Case C3: Latera in Latium region, Italy. Initial date: 15 Apr 1980. $E = 30$ *GPa*, $\nu = 0.26$, $a = 75$ *m*. Notice that in this case we have only 3 data (green). (For interpretation of the references to colour in this figure legend, the reader is referred to the web version of this article.)

affiliation with any organization with a direct or indirect financial interest in the subject matter discussed in the manuscript

Acknowledgement

The present work has been performed under the auspices of the Italian National Group for Mathematical Physics (GNFM-Indam).

References

Baisch, S., Vörös, R., Rothert, E., Stang, H., Jung, R., Schellschmidt, R., 2010. A numerical model for fluid injection induced seismicity at soultz-sous-forÕts. Int. J. Rock Mech. Min. Sci. 47 (3), 405413.

Batini, F., Bufe, C., Cameli, G.M., Console, R., Fiordelisi, A., 1980a. Seismic Monitoring in Italian Geothermal Areas I: Seismic Activity in the Larderello-travale Region. Proceedings Second DOE-ENEL Workshop on Cooperative Researchin Geothermal Energy, Report LBL-11555, Lawrence Berkeley Laboratory, Berkeley, CA, USA, October2022, p. 2047.

Batini, F., Cameli, G.M., Carabelli, E., Fiordelisi, A., 1980. Seismic Monitoring in Italian Geothermal Areas. Proceeding o Second DOE-ENEL Workshop for Cooperative Research in Geothermal Energy, Berkeley.

Batini, F., Cameli, G.M., Carabelli, E., Fiordelisi, A., 1980b. Seismic Monitoring in Italian Geothermal Areas II: Seismic Activity in the Geothermal Fields During Exploitation. Proceedings of Second DOE-ENEL Workshop on Cooperative Research in Geothermal Energy, ReportLBL-11555, Lawrence Berkeley Laboratory, Berkeley, CA, USA, October2022, p. 4885.

De Barros, L., Cappa, F., Guglielmi, Y., Duboeuf, L., Grasso, J.R., 2019. Energy of injection-induced seismicity predicted from in-situ experiments. Sci Rep 9 (4999).

Evans, K.F., Zappone, A., Kraft, T., Deichmann, N., Moia, F., 2012. A survey of the induced seismic responses to fluid injection in geothermal and CO2 reservoirs in europe. Geothermics 41, 3054.

Foulger, G.R., Wilson, M.P., Gluyas, J.G., Julian, B.R., Davies, R.J., 2018. Global review of human-induced earthquakes. Earth Sci. Rev. 178, 438514.

Gischig, V.S., Wiemer, S., 2013. A stochastic model for induced seismicity based on non-linear pressure diffusion and irreversible permeability enhancement. Geophys J Int 194 (2), 12291249.

Griffith, A.A., 1921. The phenomena of rupture and flow in solids. Philosophical Transactions, Series A 221, 163198.

Grünthal, G., 2014. Induced seismicity related to geothermal projects versus natural tectonic earthquakes and other types of induced seismic events in central europe. Geothermics 52, 2235.

Gutenberg, B., Richter, C.F., 1956. Magnitude and energy of earthquakes. Ann. Geofis. 9, 1–15.

Häring, M.O., Schanz, U., Ladner, F., Dyer, B.C., 2008. Characterisation of the basel 1 enhanced geothermal system. Geothermics 37 (5)), 469–495.

Hirschberg, S., Wiemer, S., Burgherr, P., 2015. Energy from the earth. vdf Hochschulverlag WP5.

Majer, E.L., et al., 2007. Induced seismicity associated with enhanced geothermal systems. Geothermics 36 (3), 185222.

McGarr, A., 2014. Maximum magnitude earthquakes induced by fluid injection: limits on fluid injection earthquakes. J. Geophys. Res. Solid Earth 119 (2), 10081019.

Moia, F., Angeloni, P., Cameli, G.M., Zaninetti, A., 1993. Monitoring induced seismicity around geothermal fields and reservoirs. First Egyptian Conference on Earthquake Engineering, HurgadaEgypt 110.

National Research Council, 2013. Induced seismicity potential in energy technologies. The National Academies Press, Washington, DC.

Perez, N., 2004. Fracture mechanics. Kluwer Academic Publishers.

Rothert, E., Shapiro, S., Buske, S., Bohnhoff, M., 2003. Mutual relationship between microseismicity and seismic reflectivity: case study at the german continental deep drilling site (KTB). Geophys. Res. Lett. 30 (17).

Zang, A., et al., 2014. Analysis of induced seismicity in geothermal reservoirs an overview. Geothermics 52, 621.

Zbinden, D., Rinaldi, A.P., Urpi, L., Wiemer, S., 2017. On the physics-based processes behind production-induced seismicity in natural gas fields. Journal of Geophysical Research: Solid Earth 3792–3812.

Zehnder, A.T., 2012. Fracture mechanics. Springer.